



# Precisely phase-modulated VPO catalysts with enhanced inter-phase conjunction for acrylic acid production through the condensation of acetic acid and formaldehyde



Jun Liu<sup>a</sup>, Pengcheng Wang<sup>a</sup>, Yina Feng<sup>a</sup>, Zhijia Xu<sup>a</sup>, Xinzhen Feng<sup>a,\*</sup>, Weijie Ji<sup>a,\*</sup>, Chak-Tong Au<sup>b</sup>

<sup>a</sup> Key Laboratory of Mesoscopic Chemistry, MOE, School of Chemistry and Chemical Engineering, Nanjing University, Nanjing 210023, China

<sup>b</sup> Department of Chemistry, Hong Kong Baptist University, Kowloon Tong, Hong Kong

## ARTICLE INFO

### Article history:

Received 2 February 2019

Revised 15 April 2019

Accepted 18 April 2019

### Keywords:

Vanadium phosphorus oxide

Phase-modulation

Inter-phase conjunction

Acetic acid

Formaldehyde

Condensation

Acrylic acid

## ABSTRACT

A type of precisely phase-modulated vanadium phosphorus oxides (VPOs) was fabricated for the first time by quantitatively mixing the pure phase of  $\gamma$ -VOPO<sub>4</sub>,  $\delta$ -VOPO<sub>4</sub>, and (VO)<sub>2</sub>P<sub>2</sub>O<sub>7</sub> in certain ratios through a mechanical milling approach. The resulting materials were used as catalysts for very efficient condensation of acetic acid and formaldehyde to acrylic acid as well as methyl acrylate. The modulated dual phase VPO catalyst outperforms the single-phase counterpart, and by optimizing the reaction conditions especially the contact time, we can further considerably enhance the catalyst performance. Over an optimized catalyst of  $\delta$ -VOPO<sub>4</sub>/ $\gamma$ -VOPO<sub>4</sub> (w/w, 3/1), the (AA + MA) yield of 84.2% with the equivalent (AA + MA) formation rate of 1.71 mmol·g<sup>-1</sup>·h<sup>-1</sup> or the (AA + MA) yield of 41.8% with the equivalent (AA + MA) formation rate of 4.25 mmol·g<sup>-1</sup>·h<sup>-1</sup> is achievable at 360 °C on the formaldehyde input basis. This sort of catalyst is rather durable within a period of 110 h, and fully recovered by simple air-treatment at the reaction temperature. Due to the enhanced conjunction at the interface of two phases, the surface property of phase-modulated catalyst such as the P-O bond length and surface acidity is notably modified/enhanced, accounting for the promising catalytic performance.

© 2019 Elsevier Inc. All rights reserved.

## 1. Introduction

As a versatile unsaturated organic compound, acrylic acid (AA) is widely used in manufacture of paint additives, adhesive, textile, and leather treating agents [1,2]. Furthermore, it is also extensively utilized in manufacture of industrial monomers, methyl acrylate, butyl acrylate, ethyl acrylate, 2-hydroxyethyl ester, and polymers etc. [3,4]. Currently, most of acrylic acid is produced by the conventional two-step oxidation of propylene via acrolein intermediate [5–10]. However, the feedstock of propylene is petroleum-based, and the volatility of world oil market raises a strong motivation to develop alternative route of acrylic acid production particularly from renewable raw materials [11–13]. AA generation through the condensation of acetic acid with formaldehyde is considered as a promising approach. Acetic acid is mostly fabricated via the Monsanto process (catalytic carbonylation of methanol) whereas formaldehyde is produced by the oxidation of methanol. Methanol is now obtainable in huge scale from natural gas or coal especially in North America and Asian regions. Therefore, both acetic acid and

formaldehyde becomes relatively low-priced, especially due to the overproduction capacity of acetic acid. It is highly desirable to develop new process using acetic acid as a starting material to the downstream and value-added product such as acrylic acid. In recent years, one-step condensation of acetic acid and formaldehyde to acrylic acid has received particular attention [14–17].

There are different kinds of catalysts applied for the condensation, such as basic or acidic oxides, and acid-base bi-functional oxide catalysts [18–20]. It was reported that catalysts consisting of acidic and/or basic oxides are active for the target reaction [21–23]. For example, Ai found that the condensation of formaldehyde with acetic acid/methyl acetate [24–26] or acetone [27] to acrylic acid (and its derivative) or methyl vinyl ketone can be effectively catalyzed by the V<sub>2</sub>O<sub>5</sub>-P<sub>2</sub>O<sub>5</sub> type catalysts. Ai et al. [25] reported a yield of 65% for acrylic acid and methyl acrylate (on formaldehyde input basis) in condensation of acetic acid with methanol over a V/Ti/P ternary oxide catalyst. Gogate et al. [28] observed that a methyl methacrylate yield of 10.5% (based on methyl propionate) would be achievable in the condensation of methyl propionate with formaldehyde over a V-Si-P ternary catalyst. The vanadium phosphorus oxide (VPO) catalyst is recognized as one of the most complicated catalyst systems, and many efforts

\* Corresponding authors.

E-mail addresses: [fengxinzhen1008@163.com](mailto:fengxinzhen1008@163.com) (X. Feng), [jijw@nju.edu.cn](mailto:jijw@nju.edu.cn) (W. Ji).

have been made to advance our understanding of catalyst nature in the partial oxidation of *n*-butane to maleic anhydride [29–42]. Very recently, Ivars-Barceló et al. reported the distinct functions of bulk phase, near surface, and outermost atomic layer of VPO catalysts in the oxidative dehydrogenation of ethane [43]. The VPO type catalysts have been employed for conversion of acetic acid (methyl acetate) and formaldehyde to acrylic acid (methyl acrylate) via a condensation route. Yan et al. [44] reported a AA yield of 21.9% with the selectivity of ca. 98% in the condensation of acetic acid and formaldehyde over a VPO catalyst. The supported VPO catalyst had also been investigated on the condensation of formaldehyde with carboxylic acid and the corresponding esters [19,45], as well as acetic acid/methyl acetate [46–48]. Li and coworkers recently reported the deactivation behavior on the VPO and VPO-Zr catalysts in the condensation of methyl acetate and formaldehyde [49].

In our previous studies [18,50–59], efforts were made on preparation chemistry and catalytic behaviors in partial oxidation of *n*-butane to MA over various VPO catalysts. It is obvious that the preparation history of VPO type catalyst can dramatically impact on its physicochemical properties such as phase composition, morphology, particle size, surface P/V ratio, and vanadium oxidation state. Notably, we found out that the efficient condensation of formaldehyde with acetic acid or methyl acetate can be accomplished over the controllably activated VPO catalysts using different reactors under the specific atmospheres [18], and the  $\delta$ -VOPO<sub>4</sub> phase was identified for the first time to be critical for the target reaction. In the current work, we first synthesized the VPO samples of essentially pure phase, including  $\delta$ -VOPO<sub>4</sub>,  $\gamma$ -VOPO<sub>4</sub>, and (VO)<sub>2</sub>P<sub>2</sub>O<sub>7</sub>, in a controlled way; then the phase composition of a catalyst was precisely modulated by quantifying the ratio of different pure phases. The inter-phase conjunction was further systematically tuned by mechanically ball milling various phase-modulated samples. The derived materials were subjected to calcinations under the controlled atmospheres and evaluated for the condensation of formaldehyde with acetic acid. The results demonstrated that the phase constitution and the involved inter-phase conjunction did show a significant impact on the catalytic behavior of the received materials. The highest formation rate of acrylic acid/methyl acrylate was achieved so far over the specifically phase-modulated, mechanically ball-milled, and controllably activated catalyst. The current study disclosed a successful approach to developing highly efficient VPO type catalyst and tuning unique inter-phase conjunction significant for the desired reaction pathway. Techniques including XRD, Raman, XPS, H<sub>2</sub>-TPR, NH<sub>3</sub>-/CO<sub>2</sub>-TPD, and <sup>31</sup>P magic angle spinning solid state NMR were employed to clarify the detailed catalyst characteristics and to establish the structure-performance correlation.

## 2. Experimental

### 2.1. Chemicals

The benzyl alcohol ( $\geq 99.0\%$ ), PEG-6000, vanadium pentoxide (V<sub>2</sub>O<sub>5</sub>), phosphoric acid (H<sub>3</sub>PO<sub>4</sub>, 85%), acetic acid ( $\geq 99.0\%$ ) are analytical grade. There is a small fraction of methanol (ca. 6%) existing in the commercially available formaldehyde solution (37%) serving as a stabilizing agent.

### 2.2. Catalyst preparation

The preparation of catalyst precursors was described previously [18,53]. Benzyl alcohol was employed as the preparation media. V<sub>2</sub>O<sub>5</sub> was first refluxed in benzyl alcohol at 140 °C for 5 h, after that certain amount of PEG 6000 was introduced. One hour later, phos-

phoric acid (85%) was added drop wise to reach a P/V atomic ratio being 1.05/1.0. The suspension was refluxed for another 6 h, and then the solid was filtered out, and washed with acetone. It was further dried at 100 °C in air for 24 h to obtain catalyst precursor. Before characterization and performance evaluation, all the precursors were activated according to the following procedures.

The activation of catalyst precursor was performed in a quartz tube reactor at different flowing atmospheres and temperatures to obtain distinct phase of VPO. Generally, the precursor powder of 10 g was charged into the reactor which was set in the thermostatic zone of a tubular furnace.

(a) The precursor was activated at 400 °C for 15 h under a flowing atmosphere (certain volume percentage of O<sub>2</sub> in the balanced N<sub>2</sub>, 40 mL/min) [60]. A series of VPOs comprising essentially  $\delta$ -VOPO<sub>4</sub> phase were obtained.

(b) The precursor was activated at 680 °C for 12 h under a flowing atmosphere (certain volume percentage of O<sub>2</sub> in the balanced N<sub>2</sub>, 60 mL/min) [60]. A series of VPOs consisting of essentially  $\gamma$ -VOPO<sub>4</sub> phase were obtained.

(c) The precursor was activated at 400 °C for 15 h under a flowing atmosphere (1.5 vol% *n*-butane/air, 90 mL/min) [18]. A VPO sample comprising essentially (VO)<sub>2</sub>P<sub>2</sub>O<sub>7</sub> phase was obtained.

The phase-modulated VPOs containing quantified combination of binary phases, i.e., (VO)<sub>2</sub>P<sub>2</sub>O<sub>7</sub>/ $\delta$ -VOPO<sub>4</sub>, (VO)<sub>2</sub>P<sub>2</sub>O<sub>7</sub>/ $\gamma$ -VOPO<sub>4</sub>, or  $\delta$ -VOPO<sub>4</sub>/ $\gamma$ -VOPO<sub>4</sub> with a mass ratio of 1/3, 1/1, and 3/1 respectively, were obtained through mechanical ball-milling for a certain period. In the mechanical ball-milling process, 50 little agate balls were added into a 50 mL agate jar and 25 mL cyclohexane was served as milling medium. To clarify the inter-phase conjunction over the phase-modulated VPOs subjected to mechanical ball-milling, a series of reference VPOs with the same phase constitutions were made through simple mixing, i.e.,  $\gamma$ -VOPO<sub>4</sub> and  $\delta$ -VOPO<sub>4</sub> (w/w, 1/3) or (VO)<sub>2</sub>P<sub>2</sub>O<sub>7</sub> and  $\delta$ -VOPO<sub>4</sub> (w/w, 1/1) were added into a 50 mL round-bottomed flask and 25 mL cyclohexane was added as the mixing medium. Then the mixture was stirred for 12 h followed by the same drying and activation.

### 2.3. Characterization

X-ray powder diffraction (XRD) patterns were recorded on a Philips X'Pert MPD Pro X-ray diffractometer with graphite-monochromatized Cu K $\alpha$  radiation ( $\lambda = 0.1541$  nm). Raman spectra were recorded at RT on an InVia-Reflex Raman spectrometer (laser source: 488 nm). Scanning electron microscopy (SEM) images were taken on a SEM instrument (S-4800). The <sup>31</sup>P magic angle spinning solid state NMR spectra were recorded on a Bruker AVANCE AVIII WB 400 spectrometer at a resonance frequency of 162.31 MHz with a 4 mm MAS NMR rotor, a pulse width of 20 ms, and a delay time of 5 s between scans were applied. The BET surface areas were measured on a ASAP 3020 material physical structure determinator. The samples were degassed at 573 K for 6 h, after which N<sub>2</sub> adsorption was conducted at 77 K. Hydrogen temperature-programmed reduction (H<sub>2</sub>-TPR) was carried out using a U-shaped quartz reactor. The catalyst (50 mg) was first pretreated in an Ar flow (40 mL/min) at 100 °C for 1 h. After the temperature was cooled down to room temperature (RT), the catalyst was heated from RT to 850 °C at a rate of 10 °C/min in a flow of 5% H<sub>2</sub>/Ar (v/v, flow rate = 40 mL/min), and the dehydrated effluent gas was analyzed using a thermal conductivity detector (TCD). The CuO was used as a reference to calibrate the H<sub>2</sub> consumption. X-ray photoelectron spectroscopy (XPS) measurement was performed on a PHI5000 Versa Probe instrument with Al K $\alpha$  radiation. The binding energy (BE) was calibrated against the C1s signal (284.6 eV) of contaminant carbon. Elemental surface composition was estimated based on the peak areas normalized using Wagner factors. Ammonia temperature-programmed desorption

(NH<sub>3</sub>-TPD) was carried out using a U-shaped quartz reactor. The catalyst (50 mg) was first pretreated in a He flow (40 mL/min) at 200 °C for 1 h. After the temperature was cooled down to 100 °C, NH<sub>3</sub> adsorption was performed at 100 °C for 1 h. Then, the catalyst was purged with a He flow until a steady baseline was obtained. Finally, NH<sub>3</sub>-TPD was carried out in a He flow (40 mL/min) with the sample being heated to 450 °C at a rate of 20 °C/min, and the effluent gas was analyzed by TCD. The amount of desorbed NH<sub>3</sub> (in μmol/g) was determined by a titration, in which a HCl solution (0.01 mol/L) was used to absorb the released NH<sub>3</sub>. A NaOH solution (0.01 mol/L) was used as the titrant. CO<sub>2</sub>-TPD was performed similarly and the effluent gas was analyzed by TCD.

For the V element of different oxidation state, the relative surface concentration can be estimated through deconvolution analysis of a specific XPS peak. For the same batch of sample measured employing identical conditions as well as the same parameters adopted for deconvolution analysis, comparison of the V<sup>4+</sup>/V<sup>5+</sup> ratios over different samples is reasonable. The deviation of such analysis is generally < ±5% in relative amount.

#### 2.4. Catalyst evaluation

Catalyst evaluation was carried out at atmospheric pressure. All the catalyst powders were pressed, crushed, and sieved to 20–40 mesh for activity evaluation. Two reactors were used for catalyst evaluation, one has an ID of 10 mm without a thermocouple jacket, and the other has an ID of 12 mm with a thermocouple jacket whose outside diameter is 3 mm. The reaction data derived from the two reactors were proved to be reproducible. Catalyst of 3 g was charged into the reactor, and the space above the catalyst bed was filled with quartz chips to preheat the in-coming liquid. Before feedstock introduction, the sample was heated up in a flow of N<sub>2</sub> (30 mL/min) to a desired temperature at a rate of 10 °C/min and kept at this temperature for 2.5 h. When a mixed solution of acetic acid and formaldehyde (2.5/1, n/n) was fed, a mixture of N<sub>2</sub> and air was served as carrier gas. The liquid feed rate was 1.33–6.65 mL/h (formaldehyde feed rate, 6.1–30.5 mmol/h). Under the reaction conditions, each component (acetic acid, formaldehyde, N<sub>2</sub>, and O<sub>2</sub>) exists in gaseous state and its feed concentration is indicated in vol% (mol%) together with the total gas hourly space velocity (h<sup>-1</sup>). Typically, the GHSV of 1496 h<sup>-1</sup> and feed composition of 15.3/6.1/17.3/2.2/71.5 (molar fraction) was employed. The products were collected in a cold trap. After 2.5-h reaction, the collected liquid phase was analyzed using a gas chromatograph equipped with a flame ion detector (FID) and a HP-FFAP capillary column (0.32 mm × 25 m). Valeric acid and iso-butyl alcohol were used as internal standards for component quantification. All the catalysts were first evaluated by screening their performances in terms of the (AA + MA) yield in the collected liquid sample based on formaldehyde input. Further evaluations were made on a few representative catalysts. In these circumstances, the off-gas was on-line analyzed by a GC equipped with TCD and TDX-01 packed column. It is worth noting that the formaldehyde component cannot be measured by GC analysis, therefore, the formaldehyde conversion cannot be directly determined by using the GC analysis data. In some cases, the unreacted HCHO content was analyzed by the iodometry method, to directly determine the HCHO conversion. Yield value is usually dependent upon a few parameters such as catalyst amount, concentration of reactants, gas hourly space velocity (GHSV), and time on stream (TOS). In order to minimize the influence of these parameters in comparison of catalyst activity, we generally reported the formation rate(s) for the desired product(s), namely, the amount of product(s) (in mmoles) generated on per unit mass of catalyst per hour.

Detailed examples how to determine the HCHO conversion, (AA + MA) yield/formation rate, selectivity to all the products as well as carbon balance are demonstrated in the Supplementary Material.

In our previous study [18], the issue of mass transport limitation had been studied carefully, the results indicated that the impact of internal and external diffusion was proved to be insignificant under the applied operating conditions. In the current study, the operating conditions are nearly identical to those employed in our previous study; therefore, the mass transport limitations are essentially eliminated.

### 3. Results and discussion

#### 3.1. Xrd

The XRD patterns of the VPO samples activated under various conditions plus the reference phase PDFs are shown in Fig. S1. The XRD patterns of the three single-phase VPO samples and three phase-modulated VPO samples are displayed individually with the PDF(s) of the related reference phase(s) (Fig. 1). In some cases, the phase-modulated VPO samples prepared via simple mixing and mechanical ball milling are displayed together for direct comparison (Fig. 1e–f). According to the literature works [18,60,61], the phase composition of catalyst can be significantly affected by the applied activation conditions (atmosphere and temperature). As shown in Fig. 1a, all the diffraction lines (at 2θ = 19.5°, 22.0°, 24.2°, 28.5°, etc.) are typical of the δ-VOPO<sub>4</sub> phase (PDF #47-0951), corresponding to the (0 0 2), (1 1 1), (0 1 2), and (0 2 0) plane, respectively [60]. Similarly, the diffraction lines (at 2θ = 18.1°, 22.7°, 23.2°, 25.4°, etc.) presented in Fig. 1b are typical of the γ-VOPO<sub>4</sub> phase (PDF #47-0950), corresponding to the (0 3 1), (2 2 1), (0 4 0), and (2 3 0) plane, respectively [60]. The diffraction lines (at 2θ = 23.0°, 28.4°, 29.9°, etc.) in Fig. 1c are typical of the (VO)<sub>2</sub>P<sub>2</sub>O<sub>7</sub> phase (PDF #50-0380), corresponding to the (2 0 0), (0 2 4), and (0 3 2) plane, respectively [18]. The observations indicate that nearly pure δ-VOPO<sub>4</sub>, γ-VOPO<sub>4</sub>, and (VO)<sub>2</sub>P<sub>2</sub>O<sub>7</sub> entities are obtainable when the precursors are activated under the conditions of pure O<sub>2</sub> (40 mL/min) at 400 °C, 75 vol% O<sub>2</sub>/N<sub>2</sub> (60 mL/min) at 680 °C, and 1.5 vol% n-butane/air (90 mL/min) at 400 °C, respectively. In addition, as shown in Fig. S1a, when the precursor is activated under pure O<sub>2</sub> (60 mL/min) at 680 °C, a new diffraction peak (2θ = 11.9°) appears and could be ascribed to the (0 0 1) plane of VOPO<sub>4</sub>·2H<sub>2</sub>O phase (PDF #36-1472). The oxygen rich atmosphere favors the combination of γ-VOPO<sub>4</sub> and H<sub>2</sub>O to generate VOPO<sub>4</sub>·2H<sub>2</sub>O. On the other hand, as shown in Fig. S1b, when the precursor is activated under 75 vol% O<sub>2</sub>/N<sub>2</sub> (40 mL/min) at 400 °C, a diffraction peak at 2θ = 23.0° is observed, corresponding to the (2 0 0) plane of the (VO)<sub>2</sub>P<sub>2</sub>O<sub>7</sub> phase (PDF #50-0380). In this case the oxygen concentration in the activation atmosphere is not high enough to fully oxidize the V<sup>4+</sup> species. As demonstrated in Fig. S1c and d, when the precursor is activated under pure N<sub>2</sub>, all the diffraction lines correspond to the (VO)<sub>2</sub>P<sub>2</sub>O<sub>7</sub> phase (PDF #50-0380 and 53-1051). Clearly, when the precursor is activated under an oxygen-free atmosphere, it is usually transformed into the (VO)<sub>2</sub>P<sub>2</sub>O<sub>7</sub> phase no matter when activated at 400 °C or 680 °C. When the activation atmosphere becomes oxygen-rich, the sample activated at 400 °C would comprise a high fraction of δ-VOPO<sub>4</sub> phase. If the precursor is activated in the pure oxygen, the essentially pure δ-VOPO<sub>4</sub> entity is obtained. The pure γ-VOPO<sub>4</sub> entity is obtainable when the precursor is activated under an atmosphere of 75 vol% O<sub>2</sub>/N<sub>2</sub> at a higher temperature of 680 °C.

When the pure δ-VOPO<sub>4</sub>, γ-VOPO<sub>4</sub>, and (VO)<sub>2</sub>P<sub>2</sub>O<sub>7</sub> entities are mixed with each other in certain ratios and subjected to mechanical ball milling or simple stirring, no additional diffraction lines

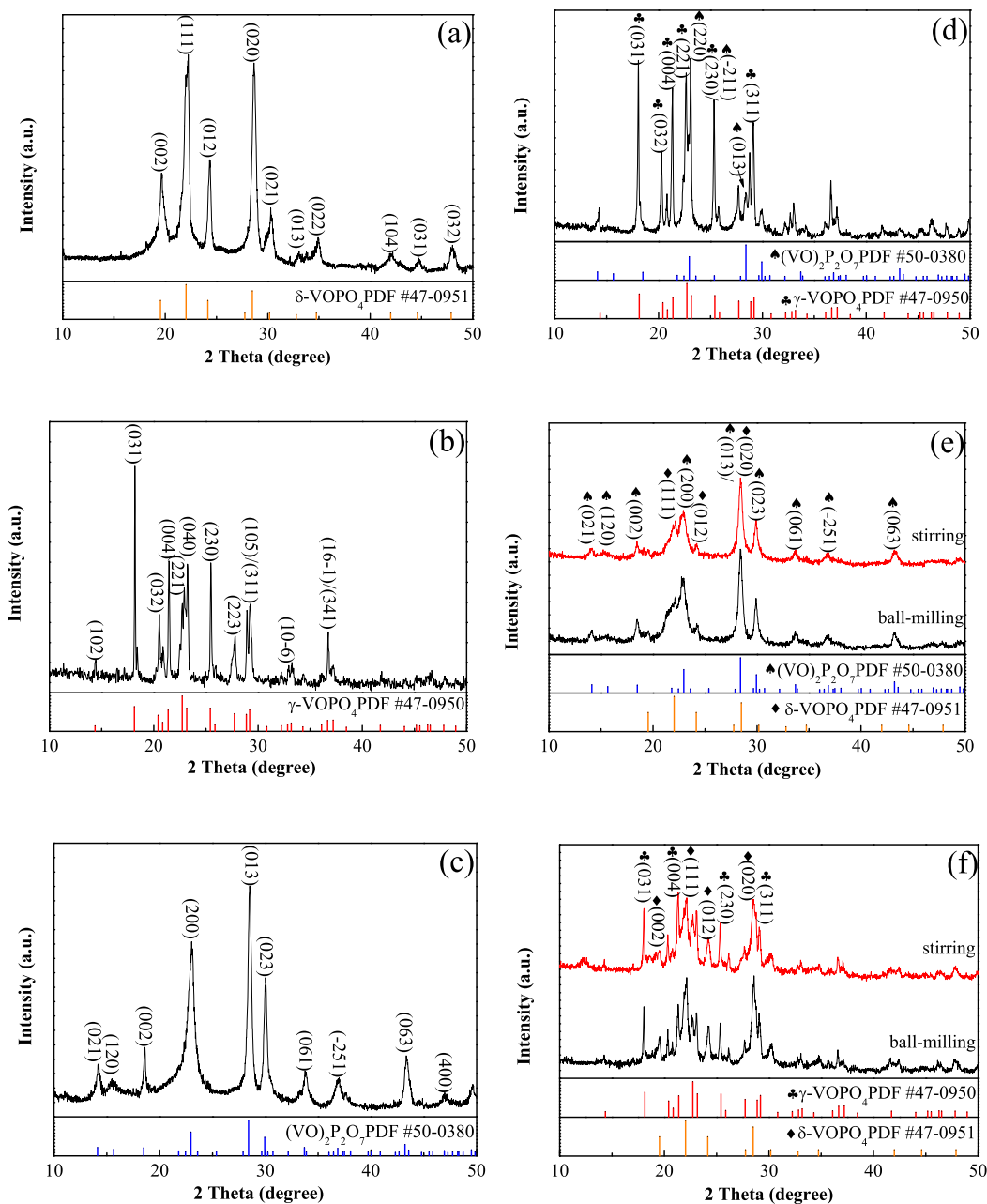


**Fig. 1.** XRD patterns of the pure phase and phase-modulated VPOs: (a)  $\delta$ -VOPO<sub>4</sub> (activated in O<sub>2</sub>, 400 °C), (b)  $\gamma$ -VOPO<sub>4</sub> (activated in 75 vol% O<sub>2</sub>/N<sub>2</sub>, 680 °C), (c) (VO)<sub>2</sub>P<sub>2</sub>O<sub>7</sub> (activated in 1.5 vol% n-butane/air, 400 °C), (d) (VO)<sub>2</sub>P<sub>2</sub>O<sub>7</sub>/ $\gamma$ -VOPO<sub>4</sub> (w/w, 1/3), (e) (VO)<sub>2</sub>P<sub>2</sub>O<sub>7</sub>/ $\delta$ -VOPO<sub>4</sub> (w/w, 1/1), (f)  $\gamma$ -VOPO<sub>4</sub>/ $\delta$ -VOPO<sub>4</sub> (w/w, 1/3).

are observed except for those of the constitutional  $\gamma$ -VOPO<sub>4</sub>,  $\delta$ -VOPO<sub>4</sub>, and (VO)<sub>2</sub>P<sub>2</sub>O<sub>7</sub> phases, suggesting that the applied mechanical ball milling or simple stirring does not alter the original phases or generate the new species. Notably, however, there are still visible differences in the diffraction intensity of ball-milled and simply stirred samples (Fig. 1e and f). For instance, in the ball-milled sample the diffraction peak of the (0 0 4) plane ( $\gamma$ -VOPO<sub>4</sub>) is more obviously weakened whereas the diffraction peak of the (1 1 1) plane ( $\delta$ -VOPO<sub>4</sub>) is considerably enhanced (Fig. 1f). The mechanical ball milling is more energetic than the simple stirring and can more effectively change the particle size and morphology, resulting in alteration of facet orientation of mixed crystallites and enhanced contact between the facets of different phases.

### 3.2. Raman

The Raman spectra of the six representative samples are demonstrated in a similar way. There are no standard Raman spectra of the single-phase VPO samples available, but as described in the experimental section, these single-phase samples are carefully synthesized according to the procedures of the literature works [18,60], and their Raman spectra are also carefully checked with respect to those reported in the same literature (Fig. 2a–c) [60]. Therefore, the character of single-phase composition of  $\delta$ -VOPO<sub>4</sub>,  $\gamma$ -VOPO<sub>4</sub>, and (VO)<sub>2</sub>P<sub>2</sub>O<sub>7</sub> samples is further confirmed. On account of the recognitions, the Raman bands of the phase-modulated VPO samples are assigned in detail (Fig. 2d–f), and the trend of phase

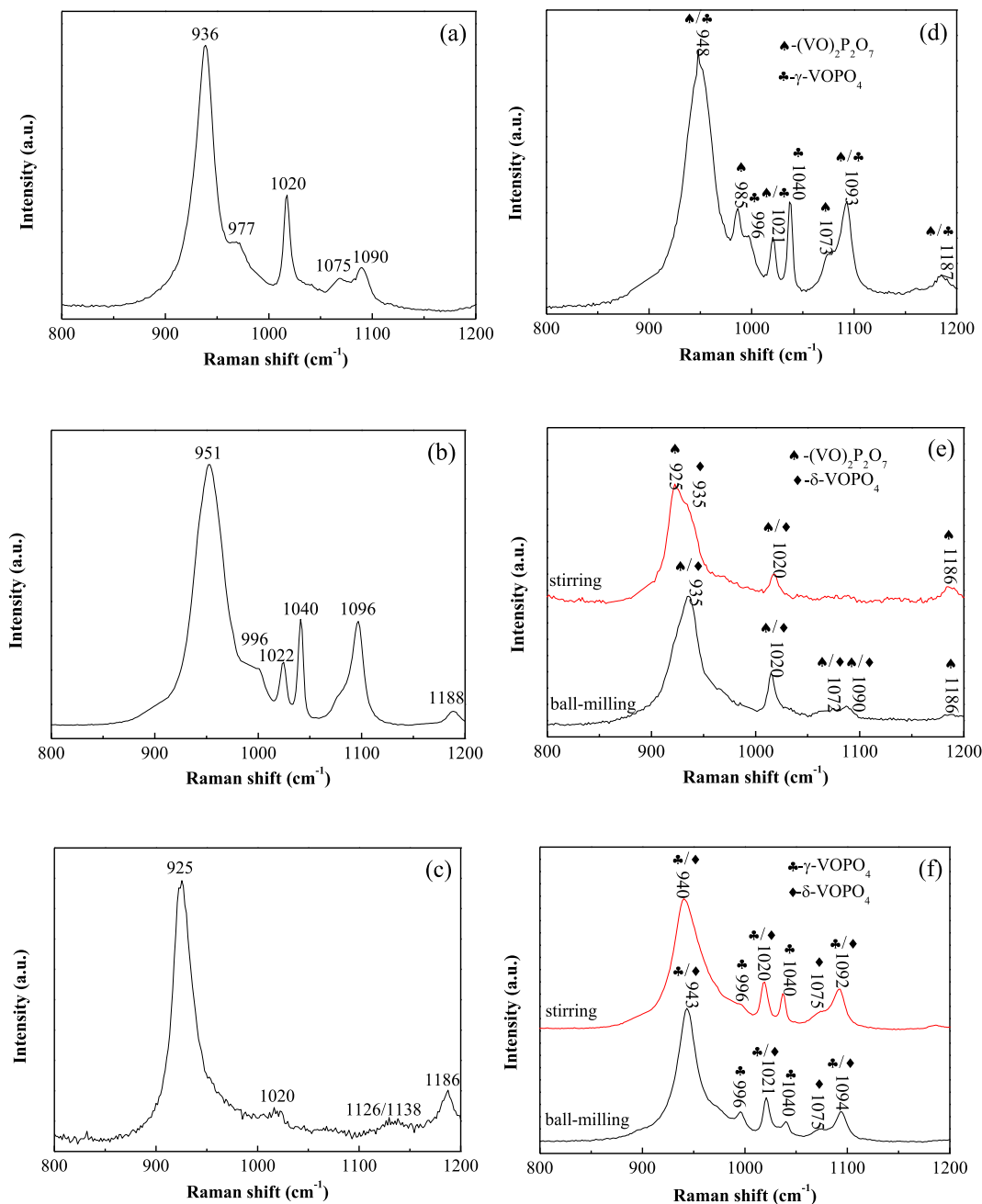


**Fig. 2.** Raman spectra of the pure phase and phase-modulated VPOs: (a)  $\delta$ -VOPO<sub>4</sub> (activated in O<sub>2</sub>, 400 °C), (b)  $\gamma$ -VOPO<sub>4</sub> (activated in 75 vol% O<sub>2</sub>/N<sub>2</sub>, 680 °C), (c) (VO)<sub>2</sub>P<sub>2</sub>O<sub>7</sub> (activated in 1.5 vol% n-butane/air, 400 °C), (d) (VO)<sub>2</sub>P<sub>2</sub>O<sub>7</sub>/ $\gamma$ -VOPO<sub>4</sub> (w/w, 1/3), (e) (VO)<sub>2</sub>P<sub>2</sub>O<sub>7</sub>/ $\delta$ -VOPO<sub>4</sub> (w/w, 1/1), (f)  $\gamma$ -VOPO<sub>4</sub>/ $\delta$ -VOPO<sub>4</sub> (w/w, 1/3).

contact/conjunction is visibly reflected in the corresponding Raman spectra (band shape change—noticeably narrower and more symmetric as well as band shift), especially when the samples subjected to simple mixing and mechanical ball milling are directly compared (Fig. 2e, f), demonstrating the generation of structurally more uniform and intensified conjunction between the two phases.

### 3.3. Xps

The surface elemental composition of the constitutional  $\gamma$ -VOPO<sub>4</sub>,  $\delta$ -VOPO<sub>4</sub>, (VO)<sub>2</sub>P<sub>2</sub>O<sub>7</sub> and the corresponding phase-modulated samples was measured by XPS. The binding energies are calibrated with respect to 284.6 eV to eliminate the impact of testing circumstance [62]. As shown in Fig. 3, the spectra (a) and

(b) only exhibit one peak whereas the spectra (c), (d), (e), and (f) can be deconvoluted into two separate components. According to the previous studies [63,64,83], the BE of V2p<sub>3/2</sub> around 516.6 eV and 517.6 eV can be assigned to that of V<sup>4+</sup> 2p<sub>3/2</sub> and V<sup>5+</sup> 2p<sub>3/2</sub>, respectively. Therefore, it is clear that the V species in the VPO catalyst activated at 680 °C under an atmosphere of 75 vol% O<sub>2</sub>/N<sub>2</sub> is in the form of V<sup>5+</sup>, whereas the V species in the VPO catalyst activated at 400 °C under an atmosphere of 1.5 vol% n-butane/air is in the form of V<sup>4+</sup>. In the case of spectrum (c), there is a minor peak at 516.0 eV, suggesting the presence of small quantity of V<sup>4+</sup> in the nearly pure  $\delta$ -VOPO<sub>4</sub> counterpart. The V<sup>4+</sup> 2p<sub>3/2</sub> and V<sup>5+</sup> 2p<sub>3/2</sub> signals can be clearly observed on spectra (d), (e) and (f).

Through the deconvolution analysis, the surface elemental composition can be estimated over the different samples and the

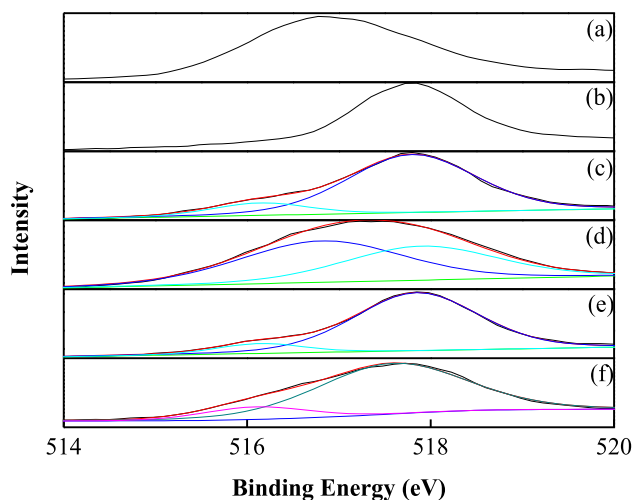


**Fig. 3.** Curve-fitting analysis of the  $V2p_{3/2}$  peaks of (a)  $(VO)_2P_2O_7$  (activated in 1.5 vol% *n*-butane/air, 400 °C), (b)  $\gamma$ - $VOPO_4$  (activated in 75 vol%  $O_2/N_2$ , 680 °C), (c)  $\delta$ - $VOPO_4$  (activated in  $O_2$ , 400 °C), (d)  $(VO)_2P_2O_7/\delta$ - $VOPO_4$  (w/w, 1/1, ball-milled), (e)  $\gamma$ - $VOPO_4/\delta$ - $VOPO_4$  (w/w, 1/3, ball-milled), and (f)  $\gamma$ - $VOPO_4/\delta$ - $VOPO_4$  (w/w, 1/3, stirred).

results are summarized in Table 1. The measured surface P/V ratios of all catalysts are found to be higher than the nominal value. This is expected because the P element is usually enriched on the VPO type catalyst [53,65,66]. Over the constitutional  $\delta$ - $VOPO_4$ , the  $V^{4+}/V^{5+}$  ratio is approximately 0.16, whereas on the constitutional  $(VO)_2P_2O_7$  and  $\gamma$ - $VOPO_4$ , neither  $V^{5+}$  in the former sample nor  $V^{4+}$  in the latter one is detectable.

### 3.4. SEM

Fig. 4 shows the typical SEM images of the constitutional  $\gamma$ - $VOPO_4$ ,  $\delta$ - $VOPO_4$ , and  $(VO)_2P_2O_7$  components and the phase-modulated samples subjected to mechanical milling. The  $\gamma$ - $VOPO_4$  entity is “rose-like” in morphology with the assembled plates of 1–2  $\mu m$  whereas the  $(VO)_2P_2O_7$  and  $\delta$ - $VOPO_4$  counterparts are irregular blocks in morphology with the particle dimension of ca. 1.5–3.5 or 1.5–4.0  $\mu m$ , respectively. On the other hand, all the phase-modulated VPO catalysts after mechanical milling exhibit fine particle in morphology with the average particle size of 0.3–0.5  $\mu m$ . The ball-milling process cracks the primary particles, thus reduces the particle size and also smoothens somewhat the particle morphology.

### 3.5. $^{31}P$ solid-state MAS NMR

The solid-state NMR spectroscopy was used to study the VPO type catalysts [67–75], because it is highly sensitive to the local structures of V/P elements. According to the literature [75], line

broadening and resonance shift occurs associating with the  $^{31}P$  solid-state NMR signals of phosphorus atoms in the proximity of paramagnetic vanadium species in VPO catalysts.

Fig. 5 shows the  $^{31}P$  solid-state MAS NMR spectra of the binary phase modulated catalysts of  $(VO)_2P_2O_7/\delta$ - $VOPO_4$  (w/w, 1/1) prepared through a mechanical milling or simple stirring. All the spectra display the main peaks at  $-17.6$  and  $-8.4$  ppm, attributable to the presence of  $\delta$ - $VOPO_4$  [60,75]. Notably, there is a small peak at around 27 ppm in spectrum (a); however, this signal is absent in spectra (b) and (c). It is supposed to be the association between P and  $V^{4+}/V^{5+}$  ions [70,76]. In other words, the applied mechanical ball-milling process of the current study enhances the  $V^{4+}$ - $V^{5+}$  interaction and also the coupling between P and  $V^{4+}/V^{5+}$  ions as a result of intensified inter-phase contact/conjunction. In terms of the catalyst activities (Section 4), the enhanced  $V^{4+}$ - $V^{5+}$  interaction caused by ball-milling process is favorable for the reaction.

Fig. 6 exhibits the  $^{31}P$  solid-state MAS NMR spectra of the binary phases modulated catalysts of  $\gamma$ - $VOPO_4/\delta$ - $VOPO_4$  (w/w, 3/1) prepared through a mechanical milling or simple stirring. According to the literature [41,58], the  $\gamma$ - $VOPO_4$  entity has two characteristic peaks at  $-21.2$  and  $-17.3$  ppm, and the  $\delta$ - $VOPO_4$  entity has two characteristic peaks at  $-17.6$  and  $-8.4$  ppm, respectively. All spectra in Fig. 5 show two main peaks at  $-13.6$  and  $-21.5$  ppm, different from that of individual  $\gamma$ - $VOPO_4$  or  $\delta$ - $VOPO_4$ . It is thought to be the result of strong coupling effect between  $\gamma$ - $VOPO_4$  and  $\delta$ - $VOPO_4$  caused by the efficient milling process. In addition, there is a shoulder at  $-9.5$  ppm in spectra (a) and (b), and it becomes more intensive in the former spectrum corresponding to an extended milling process. It is believed that this signal is closely related to the inter-phase conjunction between  $\gamma$ - $VOPO_4$  and  $\delta$ - $VOPO_4$  which is intensified by an extended milling. Note also that, the trend of signal intensity at  $-9.5$  ppm fits that of activity order (Section 4), indicating an inherent correlation between the activity and the inter-phase contact/conjunction.

### 3.6. $H_2$ -TPR

The  $H_2$ -TPR profiles over the typical catalysts were measured and the results are shown in Fig. 7. With the calibration of the reduction peak ( $H_2$  consumption), the reducibility of surface  $V^{5+}$  is estimated and the results are summarized in Table S1. Clearly, the reduction of surface  $V^{5+}/V^{4+}$  species is closely associated with the specific phase structure as well as the inter-phase conjunction especially over the phase-modulated samples.

Within the adopted temperature range, the reduction peaks centered around 500–600 °C in the TPR profiles can be attributed to the reduction of  $V^{5+}$  species, while the reduction peaks in the 700–850 °C range attributable to the reduction of  $V^{4+}$  species. Both  $\gamma$ - $VOPO_4$  and  $\delta$ - $VOPO_4$  show their reduction peaks attributable to the constitutional  $V^{5+}$  species (Fig. 7e, f) whereas the  $(VO)_2P_2O_7$  displays the major reduction peak corresponding to the constitutional  $V^{4+}$  species and almost no reduction peak appears in the

**Table 1**  
XPS data of the various VPO catalysts.

Catalyst	Relative surface concentration (at%)				P/V ratio	$V^{4+}/V^{5+}$ ratio
	C1s	V2p	P2p	O1s		
a	23.0	8.5	11.5	57.0	1.35	/
b	21.8	7.3	11.2	59.8	1.53	/
c	13.6	8.3	12.9	65.1	1.55	0.16
d	15.1	8.3	13.8	62.9	1.66	1.30
e	26.7	6.8	11.3	55.3	1.66	0.11
f	33.2	7.0	11.0	48.8	1.57	0.16

(a)  $(VO)_2P_2O_7$  (activated in 1.5 vol% *n*-butane/air at 400 °C), (b)  $\gamma$ - $VOPO_4$  (activated in 75 vol%  $O_2/N_2$  at 680 °C), (c)  $\delta$ - $VOPO_4$  (activated in  $O_2$  at 400 °C), (d)  $(VO)_2P_2O_7/\delta$ - $VOPO_4$  (w/w, 1/1, ball-milled), (e)  $\gamma$ - $VOPO_4/\delta$ - $VOPO_4$  (w/w, 1/3, ball-milled), (f)  $\gamma$ - $VOPO_4/\delta$ - $VOPO_4$  (w/w, 1/3, stirred).

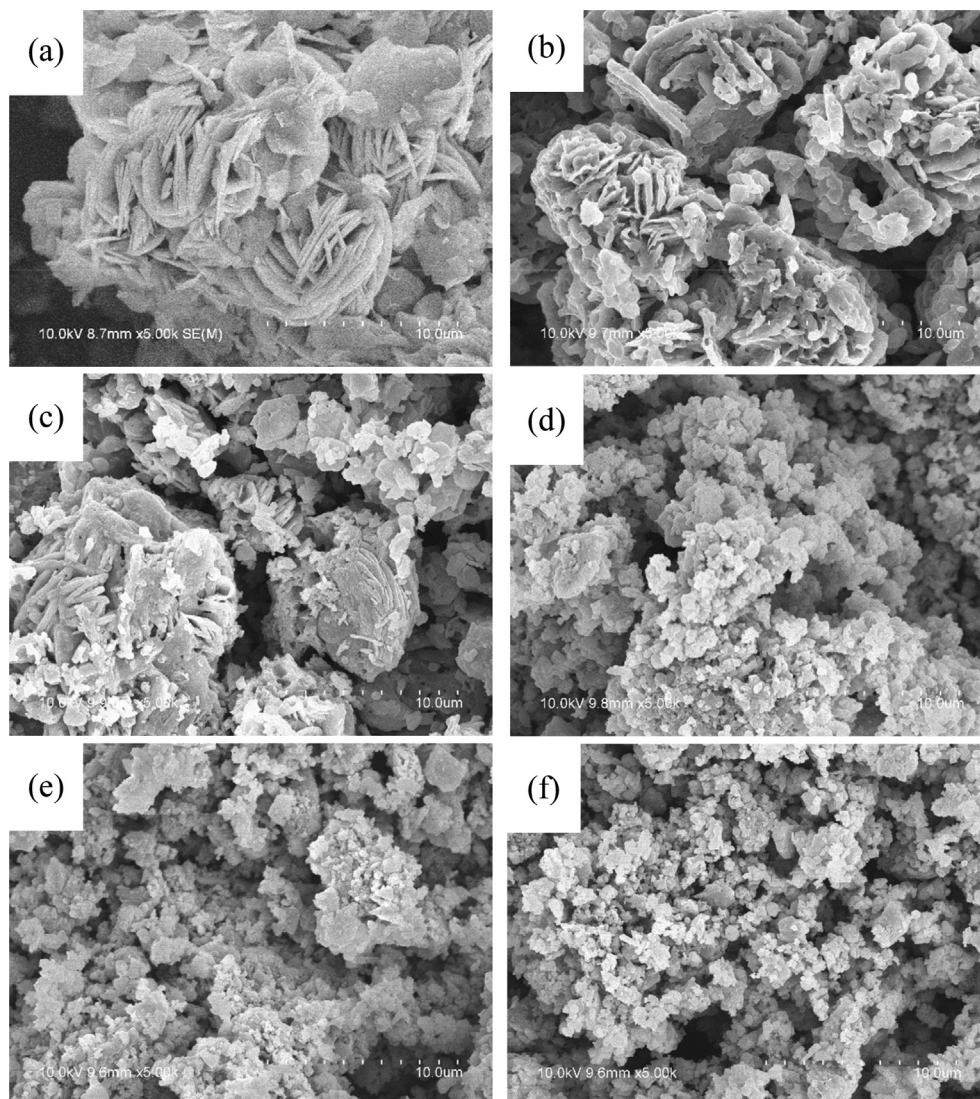


**Fig. 4.** SEM images of (a)  $(VO)_2P_2O_7$  (activated in 1.5 vol% n-butane/air, 400 °C), (b)  $\gamma\text{-VOPO}_4$  (activated in 75 vol%  $O_2/N_2$ , 680 °C), (c)  $\delta\text{-VOPO}_4$  (activated in  $O_2$ , 400 °C), (d) ball-milled  $\gamma\text{-VOPO}_4/\delta\text{-VOPO}_4$  (w/w, 1/3), (e) ball-milled  $(VO)_2P_2O_7/\delta\text{-VOPO}_4$  (w/w, 1/1), and (f) ball-milled  $(VO)_2P_2O_7/\gamma\text{-VOPO}_4$  (w/w, 1/3).

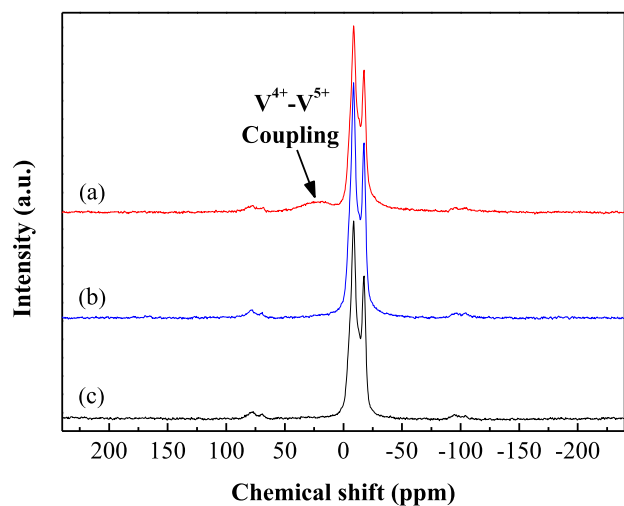


**Fig. 5.**  $^{31}P$  solid-state MAS NMR spectra of  $(VO)_2P_2O_7/\delta\text{-VOPO}_4$  (w/w, 1/1) milled or simply mixed for different time: (a) 24 h ball-milled, (b) 4 h ball-milled, and (c) 12 h simply mixed.

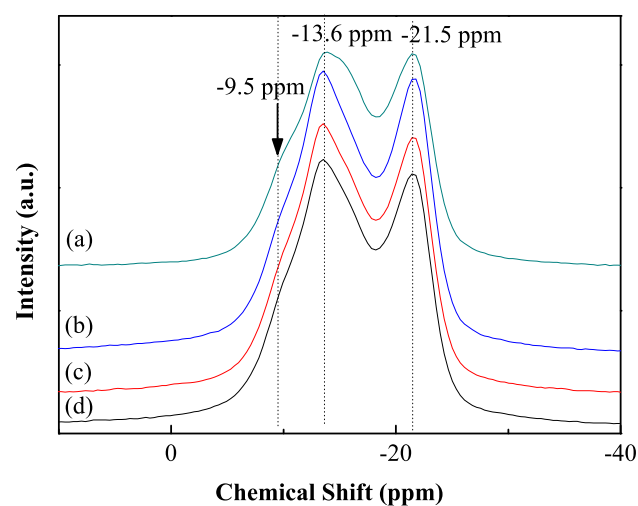


**Fig. 6.**  $^{31}P$  solid-state MAS NMR spectra of  $\gamma\text{-VOPO}_4/\delta\text{-VOPO}_4$  (w/w, 1/3) milled or simply mixed for different time: (a) 24 h ball-milled, (b) 12 h ball-milled, (c) 4 h ball-milled, and (d) 12 h simply mixed.

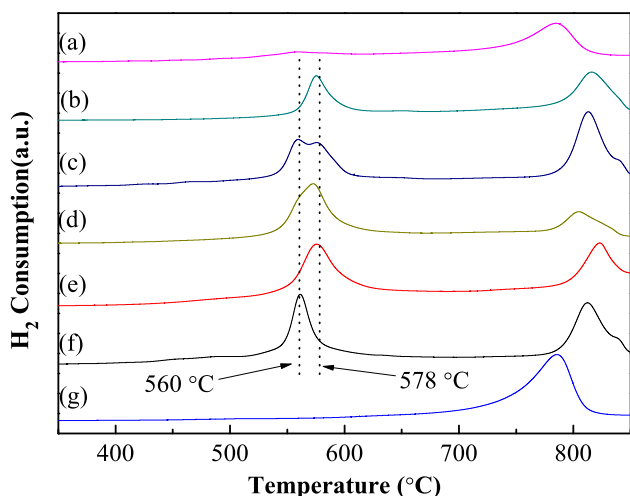


**Fig. 7.**  $H_2$ -TPR profiles of (a)  $(VO)_2P_2O_7/\delta\text{-VOPO}_4$  (w/w, 1/1, ball-milled), (b)  $(VO)_2P_2O_7/\gamma\text{-VOPO}_4$  (w/w, 1/3, ball-milled), (c)  $\gamma\text{-VOPO}_4/\delta\text{-VOPO}_4$  (w/w, 1/3, stirred), (d)  $\gamma\text{-VOPO}_4/\delta\text{-VOPO}_4$  (w/w, 1/3, ball-milled), (e)  $\gamma\text{-VOPO}_4$  (activated in 75 vol%  $O_2/N_2$ , 680 °C), (f)  $\delta\text{-VOPO}_4$  (activated in  $O_2$ , 400 °C), (g)  $(VO)_2P_2O_7$  (activated in 1.5 vol% n-butane/air, 400 °C).

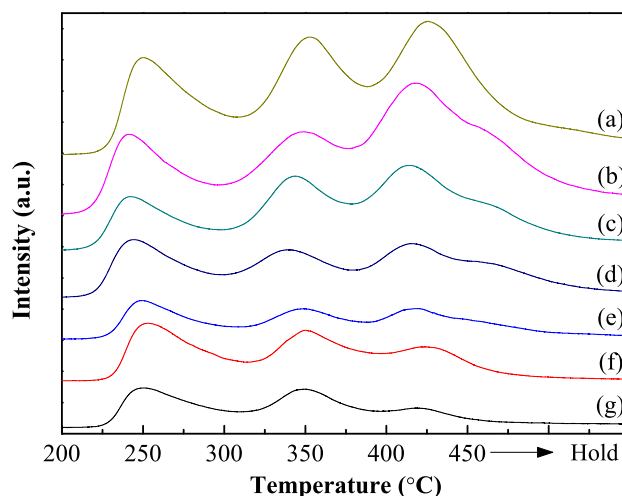


**Fig. 8.**  $NH_3$ -TPD profiles of (a)  $\gamma\text{-VOPO}_4/\delta\text{-VOPO}_4$  (w/w, 1/3, ball-milled), (b)  $(VO)_2P_2O_7/\delta\text{-VOPO}_4$  (w/w, 1/1, ball-milled), (c)  $(VO)_2P_2O_7/\gamma\text{-VOPO}_4$  (w/w, 1/3, ball-milled), (d)  $\gamma\text{-VOPO}_4/\delta\text{-VOPO}_4$  (w/w, 1/3, stirred), (e)  $(VO)_2P_2O_7$  (activated in 1.5 vol% n-butane/air, 400 °C), (f)  $\gamma\text{-VOPO}_4$  (activated in 75 vol%  $O_2/N_2$ , 680 °C), (g)  $\delta\text{-VOPO}_4$  (activated in  $O_2$ , 400 °C).

500–600 °C range (Fig. 7 g). Besides, the reduction of  $V^{5+}$  in  $\delta\text{-VOPO}_4$  and  $\gamma\text{-VOPO}_4$  occurs at different temperature (560 °C vs. 578 °C). Over the phase-modulated VPO catalysts, the reduction of  $V^{5+}$  in the constitutional phases is still distinguishable, but the behavior is influenced by the degree of inter-phase contact/conjunction. The ball milling process not only remarkably reduces the catalyst particle size but also effectively enhances the inter-phase contact (SEM images, Fig. 4d-f) and causes the structurally more uniform environment for the surface  $V^{5+}$  species to be reduced (Fig. 7c vs. d). The mechanical ball milling is more energetic than the simple stirring and can more effectively change the particle size and morphology, resulting in alteration of facet orientation of mixed crystallites and enhanced contact between the facets of different phases.

### 3.7. $NH_3/CO_2$ -Tpd

The  $NH_3$ -TPD profiles were collected over the representative catalysts and the results are shown in Fig. 8 and summarized in Table 2. Within the adopted temperature range, the desorption peaks centered around 230–240 °C are attributed to the weak acid sites, the desorption peaks centered around 340–350 °C attributable to the medium strong acid sites, and the desorption peaks centered around 430–440 °C are ascribed to the strong acid sites [46,77]. With the calibration of the corresponding  $NH_3$  desorption peak area, the acid site distribution and the total acid site density can be determined (Table 2).

Notably, the total acid site densities of the phase-modulated and ball-milled catalysts are significantly greater than that of the phase-modulated but simply-mixed counterpart as well as the single-phase catalysts. It is known that the density of medium strong acid sites on the VPO type catalyst is a crucial factor for catalytic activity. The density of medium strong acid sites shows the following order:  $\gamma\text{-VOPO}_4/\delta\text{-VOPO}_4$  (w/w, 1/3, ball-milled) >  $(VO)_2P_2O_7/\gamma\text{-VOPO}_4$  (w/w, 1/3, ball-milled) >  $\gamma\text{-VOPO}_4$  >  $(VO)_2P_2O_7/\delta\text{-VOPO}_4$  (w/w, 1/1, ball-milled) >  $\gamma\text{-VOPO}_4/\delta\text{-VOPO}_4$  (w/w, 1/3, stirred) >  $\delta\text{-VOPO}_4$  >  $(VO)_2P_2O_7$ , coincident with the trend in activity of the same catalyst serial (see below). Interestingly, the phase-modulated but simply-mixed  $\gamma\text{-VOPO}_4/\delta\text{-VOPO}_4$  (w/w, 1/3) shows remarkably lower surface acidity (especially the density of medium strong/strong as well as overall acid sites). As discussed above,

as a result of ball-milling treatment, the conjunction at the interface of two phases is enhanced, and the surface property of phase-modulated catalyst such as the P-O bond length and surface acidity can be modified accordingly, which in turn significantly improves the catalytic performance. On the other hand, in terms of the results shown in Fig. S5 and Table S11, the quantity of basic sites is much less than that of the acidic ones on the various catalysts, and there is no clear correlation observed between the catalyst basicity and the catalyst performance. Therefore, it is thought that over the current VPO type catalysts, the reaction could be mainly catalyzed by surface acidity other than basicity.

## 4. Catalytic performance

### 4.1. Effects of atmosphere and temperature for activation

The VPO samples, activated at distinct atmospheres and temperatures, were examined in aldol condensation of formaldehyde with acetic acid to AA (MA) at atmospheric pressure. The reaction temperature was 360 °C, GHSV (gas hourly space velocity) was  $1496\text{ h}^{-1}$ , with the feed composition of  $HAC/HCHO/H_2O/O_2/N_2 = 15.3/6.1/17.3/2.2/71.5$  (molar fraction) [18]. From Table S2, clearly, the atmosphere and temperature employed for activation is highly influential on catalyst performance. Regardless the activation temperature at 400 °C or 680 °C, the (AA + MA) yield increases with increasing oxygen concentration to 75 vol% in the activation atmosphere and then decreases with further increasing oxygen concentration. Hence, the optimal oxygen concentration for activation is 75%. On the other hand, the VPO activated at 680 °C is more active than the one activated at 400 °C. According to the characterization results, the catalyst activated at 400 °C consists of  $\delta\text{-VOPO}_4$  together with  $(VO)_2P_2O_7$ , and the content of  $\delta\text{-VOPO}_4$  increases with increasing oxygen concentration up to 100% at which nearly pure  $\delta\text{-VOPO}_4$  entity is obtained. Therefore, as for the  $\delta\text{-VOPO}_4$  phase, the catalytic activity is proportional to its content. Interestingly, the catalyst activated in 75%  $O_2/N_2$  is slightly better than that activated in pure oxygen, demonstrating that a mixture of major  $\delta\text{-VOPO}_4$  plus  $(VO)_2P_2O_7$  functions more favorable than nearly pure  $\delta\text{-VOPO}_4$ . In other words, the interaction between the  $\delta\text{-VOPO}_4$  and  $(VO)_2P_2O_7$  entities enhances catalytic performance, in good agreement with our previous observation [18]. Similarly, the

**Table 2**  
The surface acidity of the VPO catalysts determined by means of  $\text{NH}_3$ -TPD.

Catalyst	Acid site distribution ( $\mu\text{mol}/\text{g}_{\text{cat}}$ )			Total acid site density ( $\mu\text{mol}/\text{g}_{\text{cat}}$ )
	Weak	Medium	Strong	
a	103.5	133.8	186.2	423.5
b	89.7	74.6	236.4	400.6
c	70.6	106.2	152.6	329.3
d	76.6	68.5	107.9	252.9
e	49.3	44.4	56.1	149.8
f	85.3	93.0	63.2	241.6
g	60.3	56.1	35.7	152.2

(a)  $\gamma$ -VOPO<sub>4</sub>/ $\delta$ -VOPO<sub>4</sub> (w/w, 1/3, ball-milled), (b) (VO)<sub>2</sub>P<sub>2</sub>O<sub>7</sub>/ $\delta$ -VOPO<sub>4</sub> (w/w, 1/1, ball-milled), (c) (VO)<sub>2</sub>P<sub>2</sub>O<sub>7</sub>/ $\gamma$ -VOPO<sub>4</sub> (w/w, 1/3, ball-milled), (d)  $\gamma$ -VOPO<sub>4</sub>/ $\delta$ -VOPO<sub>4</sub> (w/w, 1/3, stirred), (e) (VO)<sub>2</sub>P<sub>2</sub>O<sub>7</sub> (activated in 1.5 vol% n-butane/air, 400 °C), (f)  $\gamma$ -VOPO<sub>4</sub> (activated in 75 vol% O<sub>2</sub>/N<sub>2</sub>, 680 °C), (g)  $\delta$ -VOPO<sub>4</sub> (activated in O<sub>2</sub>, 400 °C).

catalytic activity is closely dependent on the content of  $\gamma$ -VOPO<sub>4</sub> phase. It is worth noting that the catalyst activated in pure O<sub>2</sub> at 680 °C is less active than the one activated in 75 vol% O<sub>2</sub>/N<sub>2</sub> at 680 °C, and this is mainly due to the generation of VOPO<sub>4</sub>·2H<sub>2</sub>O species which is thought to be rather inactive for the reaction. Nevertheless, through optimizing the activation atmosphere and temperature, the phase constitution of catalyst can be tuned accordingly. The highest formation rate of 1.29 mmol·g<sup>-1</sup>·h<sup>-1</sup> for (AA + MA) is achieved among these catalysts, higher than the one previously reported by us [18].

#### 4.2. Effect of phase constitution

In Section 4.1, the catalyst phase constitution can be tuned somehow by varying activation atmosphere and temperature. However, the variation in phase constitution is not controllable, and the quantification of different phases is essentially unknown. In this section, the catalytic performances of the phase-modulated VPO catalysts have been systematically investigated. Here, the catalyst phase constitution is intentionally modulated through pre-mixing of different VPO phases [(VO)<sub>2</sub>P<sub>2</sub>O<sub>7</sub>,  $\delta$ -VOPO<sub>4</sub>, and  $\gamma$ -VOPO<sub>4</sub>] in certain ratio (w/w = 1/3, 1/1, and 3/1) followed by mechanical milling to enhance inter-phase coupling interaction. As shown in Table 3, the modulated phase constitution exhibit significant impact on catalyst performance. When (VO)<sub>2</sub>P<sub>2</sub>O<sub>7</sub> is mixed and milled with  $\gamma$ -VOPO<sub>4</sub> in different ratios, the resulting materials are superior to the individual components in activity. Clearly, the activity increases with increasing  $\gamma$ -VOPO<sub>4</sub> content, for instance, even the  $\gamma$ -VOPO<sub>4</sub> content is only 25 wt%, the (AA + MA) yield reaches 61.7%. When the  $\delta$ -VOPO<sub>4</sub> is increased to 50 wt%, the (AA + MA) yield is 63.2%, significantly higher than that on the individual (VO)<sub>2</sub>P<sub>2</sub>O<sub>7</sub> (36.8%) or  $\delta$ -VOPO<sub>4</sub> (51.5%). When the  $\delta$ -VOPO<sub>4</sub> is mixed and milled with  $\gamma$ -VOPO<sub>4</sub> in a ratio of 3:1 (w/w), the yield of (AA + MA) reaches 67.6%, corresponding to a formation rate of 1.37 mmol·g<sup>-1</sup>·h<sup>-1</sup> at 360 °C. Clearly, the dual phase-modulated

**Table 3**  
Catalytic activities of the phase-modulated catalysts subjected to ball-milling.

Catalyst	Yield of (AA + MA) (%)	(MA + AA) formation rate (mmol·g <sup>-1</sup> ·h <sup>-1</sup> )
(VO) <sub>2</sub> P <sub>2</sub> O <sub>7</sub> / $\gamma$ -VOPO <sub>4</sub> (w/w, 1/3)	66.0	1.34
(VO) <sub>2</sub> P <sub>2</sub> O <sub>7</sub> / $\gamma$ -VOPO <sub>4</sub> (w/w, 1/1)	63.4	1.29
(VO) <sub>2</sub> P <sub>2</sub> O <sub>7</sub> / $\gamma$ -VOPO <sub>4</sub> (w/w, 3/1)	61.7	1.25
(VO) <sub>2</sub> P <sub>2</sub> O <sub>7</sub> / $\delta$ -VOPO <sub>4</sub> (w/w, 1/3)	60.1	1.22
(VO) <sub>2</sub> P <sub>2</sub> O <sub>7</sub> / $\delta$ -VOPO <sub>4</sub> (w/w, 1/1)	63.2	1.28
(VO) <sub>2</sub> P <sub>2</sub> O <sub>7</sub> / $\delta$ -VOPO <sub>4</sub> (w/w, 3/1)	47.0	0.95
$\gamma$ -VOPO <sub>4</sub> / $\delta$ -VOPO <sub>4</sub> (w/w, 3/1)	63.7	1.30
$\gamma$ -VOPO <sub>4</sub> / $\delta$ -VOPO <sub>4</sub> (w/w, 1/1)	63.1	1.28
$\gamma$ -VOPO <sub>4</sub> / $\delta$ -VOPO <sub>4</sub> (w/w, 1/3)	67.6	1.37

GHSV = 1496 h<sup>-1</sup>, T = 360 °C, HAc/HCHO/H<sub>2</sub>O/O<sub>2</sub>/N<sub>2</sub> = 15.3/6.1/17.3/2.2/71.5 (molar fraction).

VPO catalysts generally outperform the unitary phase catalysts; and furthermore, the phase constitution is also critical to determine catalytic performance. The  $\gamma$ -VOPO<sub>4</sub> phase plays an important role in the reaction even if its content is in small fraction. Over a phase-modulated VPO catalyst of (VO)<sub>2</sub>P<sub>2</sub>O<sub>7</sub>/ $\delta$ -VOPO<sub>4</sub> (w/w, 1/1), its activity is enhanced most significantly, suggesting the maximum inter-phase conjunction between these two phases with similar structural feature.

In all cases, the intermediate (3-hydroxyl propanoic acid) of condensation reaction, has not been detected over the various catalysts. Moreover, we conducted the following experiments: the 3-hydroxyl propanoic acid was directly employed as a reactant and performed the reaction over the single-phase  $\delta$ -VOPO<sub>4</sub>,  $\gamma$ -VOPO<sub>4</sub>, and the phase-modulated and ball-milled  $\gamma$ -VOPO<sub>4</sub>/ $\delta$ -VOPO<sub>4</sub> (w/w, 1/3) as well as the simply mixed  $\gamma$ -VOPO<sub>4</sub>/ $\delta$ -VOPO<sub>4</sub> (w/w, 1/3) under the same operating conditions. It was found that nearly identical (AA + MA) yield was obtainable over various catalysts, suggesting that the dehydration of 3-hydroxyl propanoic acid is not a rate-determining step regarding the catalyst phase constitution, and the condensation step is more critically influenced by the enhanced conjunction over the dual phase catalyst (still phase dependent).

#### 4.3. Effect of the way of phase mixing

Catalytic performances of the dual phase-modulated VPO catalysts of (VO)<sub>2</sub>P<sub>2</sub>O<sub>7</sub>/ $\delta$ -VOPO<sub>4</sub> (w/w, 1/1) and  $\gamma$ -VOPO<sub>4</sub>/ $\delta$ -VOPO<sub>4</sub> (w/w, 1/3) through ball-milling or simple mixing are presented in Table S3. Clearly, only the ball-milled catalysts exhibit remarkably enhanced activities. Catalytic performance also increases with extended grinding time. To study the key factor for catalytic performance in the ball-milling process, the specific surface areas of the catalysts were obtained from the BET measurement and showed in Table S4. There is an order in the surface area of individual phases, namely, (VO)<sub>2</sub>P<sub>2</sub>O<sub>7</sub> >  $\delta$ -VOPO<sub>4</sub> >  $\gamma$ -VOPO<sub>4</sub>. The applied milling process considerably increases the surface area of the individual phases. However, this order is not coincident with the activity order [Table S5,  $\gamma$ -VOPO<sub>4</sub> >  $\delta$ -VOPO<sub>4</sub> > (VO)<sub>2</sub>P<sub>2</sub>O<sub>7</sub>]. Moreover, the activity of the individual phase changes insignificantly before and after milling (Table S5), suggesting that increment in surface area of individual phase show little impact on catalytic activity. Moreover, it is thought that the effective inter-phase contact and coupling interaction can only be accomplished after the ball-milling procedure and a period of 12–24 h milling is satisfactory to reduce the particle size and to intensify the inter-phase contact/conjunction.

Notably, all the phase-mixed (or phase-modulated) catalysts outperform the corresponding single-phase catalyst especially when subjected to mechanical ball milling. The ball milling process not only remarkably reduces the catalyst particle size but also effectively enhances the inter-phase contact (SEM images, Fig. 4-

d-f) and causes the structurally more uniform environment for the surface  $V^{5+}$  species ( $H_2$ -TPR profiles, Fig. 7c vs. d), leading to an enhanced conjunction at the interface of two phases (Figs. 1e, f and 2e, f). It does not mean; however, the target reaction needs a prerequisite, namely, the existence of specific conjunct interface of two phases. It is worth mentioning that, the enhanced conjunction at the interface of two phases, does have an impact on the P–O bond strength (Fig. 2f) [78], which in turn can influence on the surface acidity of catalyst and ease of the H extraction from C–H bond [79]. According to the  $NH_3$ -TPD results (Fig. 8), the density of surface acid sites is considerably increased over the phase-modulated and ball-milled samples, especially on  $\gamma$ -VOPO<sub>4</sub>/ $\delta$ -VOPO<sub>4</sub> (w/w, 1/3). Be aware of the fact that the target reaction is largely acid-catalyzed in nature (this point is interpreted in more detail below). It is true the surface region of VPO catalyst could be rather amorphous under *n*-butane oxidation, it is uncertain yet the surface state of current catalysts under the working conditions. Nevertheless, the two reactions are chemically distinct (oxidation vs. condensation), and the reaction atmosphere (1.5% *n*-butane/air vs. acetic acid/formaldehyde/water/nitrogen/oxygen) and temperature (400–420 °C vs. 360 °C) are also quite different; therefore, it is reasonably expected that for the two reactions the surface state of catalyst under the working conditions is rather incomparable and fairly dependent on the phase composition of catalyst (essentially the (VO)<sub>2</sub>P<sub>2</sub>O<sub>7</sub> for *n*-butane oxidation vs. the most effective  $\gamma$ -VOPO<sub>4</sub>/ $\delta$ -VOPO<sub>4</sub> (w/w, 1/3) for the current condensation). Even if the catalyst surface is possibly somehow structural disorder for the current system, due to the enhanced conjunction at the interface of two phases, the surface property of phase-modulated catalyst such as the P–O bond length and surface acidity is proved to be largely influenced by the original phase constitution/structure.

#### 4.4. Effects of operating parameters

The effects of reaction temperature, gas hourly space velocity, and feed condition on (AA + MA) yield and formation rate were investigated over  $\delta$ -VOPO<sub>4</sub>/ $\gamma$ -VOPO<sub>4</sub> (w/w, 3/1) and the results are shown in Table S6–S8. From Table S6, at 340 °C, the (AA + MA) yield and formation rate declines to 49.2% and 1.00 mmol·g<sup>-1</sup>·h<sup>-1</sup>, respectively. As the temperature is raised to 380 °C, the catalyst performance changes insignificantly compared to the values obtained at 360 °C. Thus 360 °C is a suitable temperature for the reaction.

The data presented in Table S7 indicate that the carrier flow rate shows dramatic impact on activity. The carrier flow rate was controlled by the  $N_2$  flow rate and the other flow rates (HAc, HCHO,  $H_2O$ , and  $O_2$ ) were remained, as the carrier flow rate is increased from 30 mL/min to 40 mL/min, the (AA + MA) yield increases from 67.6% to 84.2%, corresponding to a formation rate as high as 1.71 mmol·g<sup>-1</sup>·h<sup>-1</sup>. If the carrier flow rate is further increased to 50 mL/min, the (AA + MA) yield changes little. So a flow rate of 40 mL/min for the carrier is appropriate for the reaction. It appears that the contact time is critical to determine the selective formation of AA and MA. On one hand, prompt desorption of AA/MA from catalyst surface avoids further disintegration of the desired products; and on the other hand, quick recover of surface sites speeds up the reaction cycles [70].

The influence of feed rate on catalytic performance was also studied (Table S8). As the feed rate (based on HCHO) varies from 6.1 to 30.5 mmol·h<sup>-1</sup>, the formation rate of (AA + MA) increases steadily, meanwhile the yield of (AA + MA) declines simultaneously. At a feed rate of 18.3 mmol·h<sup>-1</sup>, the (MA + AA) formation rate reaches a level of 3.29 mmol·g<sup>-1</sup>·h<sup>-1</sup>, corresponding to a yield of (AA + MA) being 54%. At the highest feed rate (30.5 mmol·h<sup>-1</sup>) employed, the (MA + AA) formation rate and yield is 4.25 mmol·g<sup>-1</sup>·h<sup>-1</sup> and 41.8%, respectively.

#### 4.5. Correlation between characterization and evaluation results

The data of HCHO conversion and selectivity to (AA + MA) as well as all the by-products measured over the seven representative catalysts are presented in Table S12 where the total carbon balances are also included for reference.

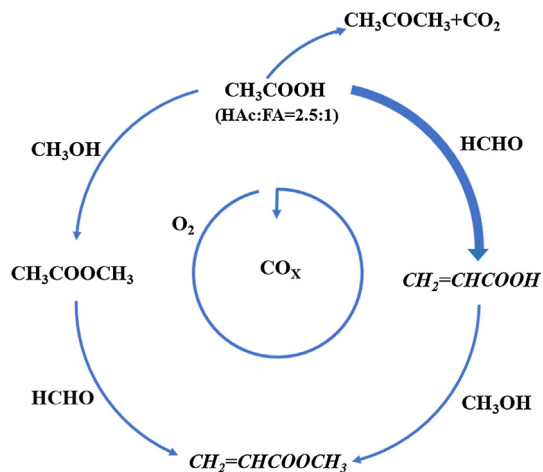
Table S13 summarizes the (AA + MA) yield, formation rate, selectivity, together with the  $V^{4+}/V^{5+}$  ratio as well as the density of medium strong acid sites. The (AA + MA) yield is closely related to the density of medium strong acid sites of catalyst which is dependent on the phase constitution of catalyst. Therefore, the phase constitution of catalyst largely impacts on the density of medium strong acid sites on the current catalysts, and the latter is crucial to determine the catalyst performance. As the activity is normalized to per surface area of catalyst, one can observe that the area-normalized (AA + MA) formation rate is comparable over catalysts b, c, e, and f except for catalysts a and d, suggesting that the surface area is also an influential factor on catalytic activity. It is worth noting that the selectivity to (AA + MA) is enhanced over the phase-modulated and ball-milled catalysts especially on VOPO<sub>4</sub>/ $\delta$ -VOPO<sub>4</sub> (w/w, 1/3), demonstrating that the ball-milling process not only efficiently increases catalyst surface area but also enhances the formation of the desired products. A comparison between catalysts e and f with originally identical phase constitution clearly indicates that the applied ball-milling enhances the inter-phase conjunction (also verified by the Raman,  $H_2$ -TPR, and solid-state MAS NMR investigations), which in turn results in a significant increment in the density of medium strong acid sites and a more selective reaction. Furthermore, there seems a direct correlation between the  $V^{4+}/V^{5+}$  ratio and the catalytic behavior. Basically, the  $V^{5+}$  looks more favorable than  $V^{4+}$  for the reaction. The presence of  $V^{4+}$  impacts slightly on selectivity but more noticeably on (AA + MA) formation rate. This is also confirmed by the deactivation behavior of catalyst: the yield of (AA + MA) continuously decreases while the corresponding selectivity changes insignificantly with time on stream, accompanying by the continuous reduction of surface  $V^{5+}$  to  $V^{4+}$  during the reaction course.

#### 4.6. The reaction scheme

The involved reactions are demonstrated in Scheme 1 regarding the fed substances in the reaction and the measured products distribution. The major reaction route is the condensation between acetic acid and formaldehyde to AA which can further react with methanol to MA. There are minor reaction routes from acetic acid plus methanol to methyl acetate which can also react with formaldehyde to MA. Acetic acid itself can subject to a side reaction to produce acetone/ $CO_2$ , but this route is found to be very limited on our catalysts. The  $CO_x$  is resulted from the deep oxidation of reactants/products.

### 5. Catalyst durability

This reaction through a continuous gas phase heterogeneous process has been studied so far by a few research groups [14,18,80,81], and in most cases, only the initial activities (2.5 h reaction period or even shorter) were reported and compared. According to the limited examples of durability tests reported by others and us [18,44], there is continuous decline in activity with time on stream regardless the deactivation is relatively slow or fast. The phase composition of VPO catalyst could be variable upon operating conditions such as reaction atmosphere and temperature. We selected the most efficient catalyst [ $\delta$ -VOPO<sub>4</sub>/ $\gamma$ -VOPO<sub>4</sub> (w/w, 3/1)] as the representative system to conduct durability test for approximately 110 h, with the GHSV of 1823 h<sup>-1</sup> and feed com-



**Scheme 1.** A reaction scheme in terms of the fed substances in the reaction and the measured products distribution. The thick arrow line corresponds to the major reaction route whereas the thin arrow lines refer to the minor reaction routes.

position being HAc/HCHO/H<sub>2</sub>O/O<sub>2</sub>/N<sub>2</sub> = 15.3/6.1/17.3/2.2/96.0 (in molar fraction, Fig. 9). The initial activity is the highest known to date and the deactivation is comparatively slower during 110 h and can be fully recovered by simple air-treatment at the reaction temperature.

To verify the possible phase variation of catalyst during the reaction period, the used catalyst subjected to different reaction period (2.5 h, 27 h, and 72 h, respectively) and regeneration was collected and analyzed by means of Raman, XPS, and NH<sub>3</sub>-TPD. The reaction performances are listed in Table S9 and the characterization results are presented in Figs. S2–S4 and Table S10. Notably, the HCHO conversion gradually decreases with time on stream. However, the selectivity for target products essentially retains (the inset of Fig. 9), suggesting that the deactivation is associated to the decrease in conversion rather than selectivity. As demonstrated in Figs. S2 and S3, over the used sample (72 h), the Raman band of  $\nu_s$  (P–O) shifts to 932 cm<sup>-1</sup> [(VO)<sub>2</sub>P<sub>2</sub>O<sub>7</sub>] and the surface V<sup>5+</sup> is mostly reduced to V<sup>4+</sup>. Over the regenerated catalyst, the Raman band of  $\nu_s$  (P–O) shifts back to 941 cm<sup>-1</sup> and the surface V<sup>4+</sup>/V<sup>5+</sup> ratio is recovered to 0.60 (Table S10), indicating that in the surface region of catalyst, the V<sup>5+</sup> species in the original  $\delta$ -VOPO<sub>4</sub>/ $\gamma$ -VOPO<sub>4</sub> phases is gradually reduced to V<sup>4+</sup> species [(VO)<sub>2</sub>P<sub>2</sub>O<sub>7</sub>-like entity]

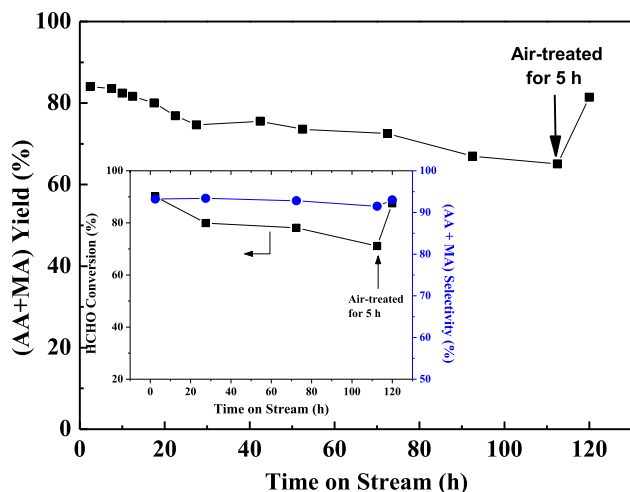


**Fig. 9.** Durability test over  $\gamma$ -VOPO<sub>4</sub>/ $\delta$ -VOPO<sub>4</sub> (w/w, 1/3) at 360 °C for a period of approximately 120 h.

with time on stream, and such evolution of V oxidation state is reversible upon air-treatment. Interestingly, accompanying with the variation in V oxidation state, the density of weak/medium strong acid sites decreases accordingly and is significantly recovered upon regeneration (Fig. S4). These characterization findings over the used catalysts of different period reasonably account for the variation in catalytic performance with time on stream up to 120 h. It is worth noting that the catalytic performance is not simply determined by the reducibility of  $\delta$ -VOPO<sub>4</sub> or  $\gamma$ -VOPO<sub>4</sub> phase. According to Fig. 7, although  $\gamma$ -VOPO<sub>4</sub> is more difficult to reduce than  $\delta$ -VOPO<sub>4</sub>, the single  $\gamma$ -VOPO<sub>4</sub> is obviously inferior to the phase-modulated  $\delta$ -VOPO<sub>4</sub>/ $\gamma$ -VOPO<sub>4</sub> (w/w, 3/1) in catalytic performance, suggesting the phase-coupling is critical in determining catalytic activity.

To verify whether there is V<sup>3+</sup> species existing in the fresh and used catalysts, the representative catalyst of  $\gamma$ -VOPO<sub>4</sub>/ $\delta$ -VOPO<sub>4</sub> (w/w, 1/3, ball-milled) was first subjected to a H<sub>2</sub>-TPR procedure (from RT to 850 °C) and then analyzed by XPS. As shown in Fig. S6a, there is one peak centered at 515.8 eV attributable to V<sup>3+</sup> 2p<sub>3/2</sub> [82], confirming that the V<sup>3+</sup> is dominated after the H<sub>2</sub>-TPR procedure. Over the same catalyst used for 72 h (Fig. S6b), though V<sup>4+</sup> is dominant on the catalyst surface, a small quantity of V<sup>3+</sup> can also be identified. In contrast, the fresh catalyst (Fig. S6c) shows the two deconvoluted peaks at 516.6 and 517.6 eV, corresponding to V<sup>4+</sup> 2p<sub>3/2</sub> and V<sup>5+</sup> 2p<sub>3/2</sub>, respectively [63,64]. Therefore, it is clarified that the V<sup>3+</sup> species are essentially undetectable on the fresh catalyst surface, but could be detected in a low content on the used catalyst surface with a TOS of 72-h.

## 6. Concluding remarks

In this study, the precisely phase-modulated VPO catalysts were fabricated and the inter-phase conjunction can be effectively enhanced by the approach of mechanical grinding and controlled activation. The resulting materials were applied for the gas phase condensation of acetic acid and formaldehyde to acrylic acid (methyl acrylate). The present work is the first example to demonstrate the significance of quantification of VPO phase constitution in determining catalyst performance for the target reaction. Systematic characterizations reveal the important information on the phase type of VPO component, the surface concentration and oxidation state of V element, the surface V/P ratio, the redox behavior, and the surface acidity of unitary phase and dual phase-modulated catalysts. Through systematic tuning the phase type and constitution as well as the activation conditions, we obtained the most efficient VPO catalyst system so far for the target reaction. Over an optimized catalyst of  $\delta$ -VOPO<sub>4</sub>/ $\gamma$ -VOPO<sub>4</sub> (w/w, 3/1), the (AA + MA) yield of 84.2% with the equivalent (AA + MA) formation rate of 1.71 mmol·g<sup>-1</sup>·h<sup>-1</sup> or the (AA + MA) yield of 41.8% with the equivalent (AA + MA) formation rate of 4.25 mmol·g<sup>-1</sup>·h<sup>-1</sup> are achievable on the formaldehyde input basis under the controlled conditions. This sort of catalyst can be reproducibly fabricated, rather durable within a period of 110 h, and fully recovered by simple air-treatment at the reaction temperature.

## Acknowledgement

The financial support of National Nature Science Foundation of China (21673112) is greatly appreciated.

## Appendix A. Supplementary material

Supplementary data to this article can be found online at <https://doi.org/10.1016/j.jcat.2019.04.032>.

## References

- [1] H. Danner, M. Neureiter, L. Madzingaidzo, M. Gartner, R. Braun, *Appl. Biochem. Biotechnol.* 70 (1998) 895–903.
- [2] X.B. Xu, J.P. Lin, P.L. Cen, *Chin. J. Chem. Eng.* 14 (2006) 419–427.
- [3] P.T. Anastas, J.C. Warner, *Green Chemistry: Theory and Practice*, Oxford University Press, New York, 1998, pp. 11–56.
- [4] C.C. Zuo, Y.P. Li, C.S. Li, S.S. Cao, H.Y. Yao, S.J. Zhang, *AlChE J.* 62 (2016) 228–240.
- [5] M.M. Lin, *Appl. Catal., A* 207 (2001) 1–16.
- [6] X.J. Yang, R.M. Feng, W.J. Ji, C.-T. Au, *J. Catal.* 253 (2008) 57–65.
- [7] N. Mizuno, M. Tateishi, M. Iwamoto, *Appl. Catal., A* 128 (1995) L165–L170.
- [8] U. Takashi, N. Hiroya, K. Yukio, W. Shin, *US Patent 5380933*, 1995.
- [9] M.M. Lin, *Appl. Catal., A* 250 (2003) 305–318.
- [10] P. Botella, J.M. López Nieto, B. Solsona, A. Mifsud, F. Márquez, *J. Catal.* 209 (2002) 445–455.
- [11] W. Fang, Q.J. Ge, J.F. Yu, H.Y. Xu, *Ind. Eng. Chem. Res.* 50 (2011) 1962–1967.
- [12] R.N. d'Aloncourt, L.-I. Csepei, M. Hävecker, F. Girgsdies, M.E. Schuster, R. Schlögl, A. Trunschke, *J. Catal.* 311 (2014) 369–385.
- [13] B.Y. Jo, S.S. Kum, S.H. Moon, *Appl. Catal., A* 378 (2010) 76–82.
- [14] M. Ai, *J. Catal.* 107 (1987) 201–208.
- [15] O.H. Bailey, R.A. Montag, J.S. Yoo, *Appl. Catal., A* 88 (1992) 163–177.
- [16] M. Ai, H. Fujihashi, S. Hosoi, A. Yoshida, *Appl. Catal., A* 252 (2003) 185–191.
- [17] J.R. Tai, R.J. Davis, *Catal. Today* 123 (2007) 42–49.
- [18] X.Z. Feng, B. Sun, Y. Yao, Q. Su, W.J. Ji, C.-T. Au, *J. Catal.* 314 (2014) 132–141.
- [19] M. Ai, *Appl. Catal., A* 288 (2005) 211–215.
- [20] J.B. Yan, C.L. Zhang, C.L. Ning, Y. Tang, Y. Zhang, L.L. Chen, S. Gao, Z.L. Wang, W. X. Zhang, *J. Ind. and Eng. Chem.* 25 (2015) 344–351.
- [21] R.K. Zeidan, M.E. Davis, *J. Catal.* 247 (2007) 379–382.
- [22] B. Liu, S.J. Wu, X.F. Yu, J.Q. Guan, Q.B. Kan, *J. Colloid Interface Sci.* 362 (2011) 625–628.
- [23] B. Li, R.Y. Yan, L. Wang, Y.Y. Diao, Z.X. Li, S.J. Zhang, *Catal. Lett.* 143 (2013) 829–838.
- [24] M. Ai, *J. Catal.* 112 (1988) 194–200.
- [25] M. Ai, *Appl. Catal.* 59 (1990) 227–235.
- [26] M. Ai, *Stud. Surf. Sci. Catal.* 72 (1992) 101–108.
- [27] M. Ai, *J. Catal.* 106 (1987) 273–279.
- [28] M.R. Gogate, J.J. Spivey, J.R. Zoeller, *Catal. Today* 36 (1997) 243–254.
- [29] B.K. Hodnett, *Cat. Rev. Sci. Eng.* 27 (1985) 373–424.
- [30] G. Centi, F. Trifiro, J.R. Ebner, V.M. Franchetti, *Chem. Rev.* 88 (1988) 55–80.
- [31] G.J. Hutchings, A. Desmartin-Chomel, R. Olier, J.C. Volta, *Nature* 368 (1994) 41–45.
- [32] R. Nilsson, T. Lindblad, A. Andersson, *J. Catal.* 148 (1994) 501–513.
- [33] M.T. Sananes, G.J. Hutchings, J.C. Volta, *J. Catal.* 154 (1995) 253–260.
- [34] C.J. Kiely, A. Burrows, G.J. Hutchings, K.E. Bere, J.C. Volta, A. Tuel, M. Abon, *Faraday Discuss.* 105 (1996) 103–118.
- [35] S. Albonetti, F. Cavani, F. Trifirò, *Cat. Rev. Sci. Eng.* 38 (1996) 413–438.
- [36] G.W. Coulston, S.R. Bare, H. Kung, K. Birkeland, G.K. Bethke, R. Harlow, N. Herron, P.L. Lee, *Science* 275 (1997) 191–193.
- [37] J.M. Herrmann, P. Vernoux, K.E. Béré, M. Abon, *J. Catal.* 167 (1997) 106–117.
- [38] V.V. Gulians, S.A. Holmes, J.B. Benziger, P. Heaney, D. Yates, I.E. Wachs, *J. Mol. Catal. A: Chem.* 172 (2001) 265–276.
- [39] G.J. Hutchings, J.A. Lopez-Sanchez, J.K. Bartley, J.M. Webster, A. Burrows, C.J. Kiely, A.F. Carley, C. Rhodes, M. Hävecker, A. Knop-Gericke, R.W. Mayer, R. Schlögl, J.C. Volta, M. Poliakoff, *J. Catal.* 208 (2002) 197–210.
- [40] N. Hiyoshi, N. Yamamoto, N. Ryumon, Y. Kamiya, T. Okuhara, *J. Catal.* 221 (2004) 225–233.
- [41] M. Conte, G. Budroni, J.K. Bartley, S.H. Taylor, A.F. Carley, A. Schmidt, D.M. Murphy, F. Girgsdies, T. Ressler, R. Schlögl, G.J. Hutchings, *Science* 313 (2006) 1270–1273.
- [42] J.K. Bartley, N.F. Dummer, G.J. Hutchings, Vanadium phosphate catalysts metal oxide catalysis, in: S.D. Jackson, J.S.J. Hargreaves (Eds.), *WILEY-VCH Verlag, Weinheim*, 2009 (Chapter 12).
- [43] F. Ivars-Barceló, G.J. Hutchings, J.K. Bartley, S.H. Taylor, P. Sutter, P. Amorós, R. Sanchis, B. Solsona, *J. Catal.* 354 (2017) 236–249.
- [44] D. Yang, C. Sararuk, K. Suzuki, Z.X. Li, C.S. Li, *Chem. Eng. J.* 300 (2016) 160–168.
- [45] M. Ai, *Stud. Surf. Sci. Catal.* 162 (2006) 457–464.
- [46] D. Yang, C. Sararuk, H. Wang, S.J. Zhang, Z.X. Li, C.S. Li, *Ind. Eng. Chem. Res.* 57 (2018) 93–100.
- [47] H. Zhao, C.C. Zuo, D. Yang, C.S. Li, S.J. Zhang, *Ind. Eng. Chem. Res.* 55 (2016) 12693–12702.
- [48] D. Yang, D. Li, H.Y. Yao, G.L. Zhang, T.T. Jiao, Z.X. Li, C.S. Li, S.J. Zhang, *Ind. Eng. Chem. Res.* 54 (2015) 6865–6873.
- [49] D. Yang, G. Wang, H. Wu, X.P. Guo, S.J. Zhang, Z.X. Li, C.S. Li, *Catal. Today* 316 (2018) 122–128.
- [50] X. Feng, Y. Yao, Q. Su, L. Zhao, W. Jiang, W.J. Ji, C.-T. Au, *Appl. Catal., B* 164 (2015) 31–39.
- [51] X.S. Wang, W.Y. Nie, W.J. Ji, X.F. Guo, Q.J. Yan, Y. Chen, *Chem. Lett.* 30 (2001) 696–697.
- [52] W.J. Ji, L.J. Xu, X.S. Wang, Z. Hu, Q.J. Yan, Y. Chen, *Catal. Today* 74 (2002) 101–110.
- [53] X.S. Wang, L.J. Xu, X. Chen, W.J. Ji, Q.J. Yan, Y. Chen, *J. Mol. Catal. A: Chem.* 206 (2004) 261–268.
- [54] W.Y. Nie, Z.Y. Wang, W.J. Ji, Y. Chen, C.-T. Au, *Appl. Catal., A* 244 (2003) 265–272.
- [55] C.Y. Xiao, X. Chen, Z.Y. Wang, W.J. Ji, Y. Chen, C.-T. Au, *Catal. Today* 93–95 (2004) 223–228.
- [56] Z.Q. Zhou, H.Y. Xu, W.J. Ji, Y. Chen, *Catal. Lett.* 96 (2004) 221–226.
- [57] X.K. Li, W.J. Ji, J. Zhao, Z.B. Zhang, C.-T. Au, *J. Catal.* 238 (2006) 232–241.
- [58] R.M. Feng, X.J. Yang, W.J. Ji, Y. Chen, C.-T. Au, *J. Catal.* 246 (2007) 166–176.
- [59] Q. Jiang, J. Zhao, X.K. Li, W.J. Ji, Z.B. Zhang, C.-T. Au, *Appl. Catal., A* 341 (2008) 70–76.
- [60] F. Ben Abdelouahab, R. Olier, N. Guilhaume, F. Lefebvre, J.C. Volta, *J. Catal.* 134 (1992) 151–167.
- [61] T.P. Moser, G.L. Schrader, *J. Catal.* 92 (1985) 216–231.
- [62] E. Bordes, *Catal. Today* 1 (1987) 499–526.
- [63] P.T. Nguyen, R.D. Hoffman, A.W. Sleight, *Mater. Res. Bull.* 30 (1995) 1055–1063.
- [64] F.D. Hardcastle, I.E. Wachs, *J. Phys. Chem.* 95 (1991) 5031–5041.
- [65] Y. Jia, D.Q. Du, J.C. Bai, J. Ding, Q. Zhong, X.L. Ding, *Atmos. Pollut. Res.* 6 (2015) 184–190.
- [66] M.J. Cheng, W.A. Goddard, *J. Am. Chem. Soc.* 135 (2013) 4600–4603.
- [67] B.M. Reddy, I. Ganesh, E.P. Reddy, *J. Phys. Chem. B* 101 (1997) 1769–1774.
- [68] V.I. Bukhtiyarov, *Catal. Today* 56 (2000) 403–413.
- [69] J. Kasperkiewicz, J.A. Kovacic, D. Lichtman, *J. Electron. Spectrosc. Relat. Phenom.* 32 (1983) 123–132.
- [70] R.A. Overbeek, A.R.C.J. Pikelharing, A.J. van Dillen, J.W. Geus, *Appl. Catal., A* 135 (1996) 231–248.
- [71] R.A. Overbeek, P.A. Warringa, M.J.D. Crombag, L.M. Visser, A.J. van Dillen, J.W. Geus, *Appl. Catal., A* 135 (1996) 209–230.
- [72] J. Li, M.E. Lashier, G.L. Schrader, B.C. Gerstein, *Appl. Catal.* 73 (1991) 83–95.
- [73] M.T. Sananes, A. Tuel, J.C. Volta, *J. Catal.* 145 (1994) 251–255.
- [74] M.T. Sananes, A. Tuel, *Solid State Nucl. Magn. Reson.* 6 (1996) 157–166.
- [75] K.E. Birkeland, S.M. Babitz, G.K. Bethke, H.H. Kung, G.W. Coulston, S.R. Bare, *J. Phys. Chem. B* 101 (1997) 6895–6902.
- [76] M.T. Sananes-Schulz, A. Tuel, G.J. Hutchings, J.C. Volta, *J. Catal.* 166 (1997) 388–392.
- [77] A. Tuel, M.T. Sananes-Schulz, J.C. Volta, *Catal. Today* 37 (1997) 59–68.
- [78] O.B. Lapina, D.F. Khabibulin, A.A. Shubin, V.M. Bondareva, *J. Mol. Catal. A: Chem.* 162 (2000) 381–390.
- [79] V. Robert, S. Petit, S.A. Borshch, B. Bigot, *J. Phys. Chem. A* 104 (2000) 4586–4591.
- [80] J. Frey, C. Lieder, T. Schölkopf, T. Schleid, U. Nieken, E. Klemm, M. Hunger, *J. Catal.* 272 (2010) 131–139.
- [81] N.H. Batis, H. Batis, A. Ghorbel, J.C. Vedrine, J.C. Volta, *J. Catal.* 128 (1991) 248–263.
- [82] B. Horvath, J. Strutz, J. Geyer-Lippmann, E.G. Horvath, *Z. Anorg. Allg. Chem.* 483 (1981) 181–192.
- [83] T.P. Moser, G.L. Schrader, *J. Catal.* 104 (1987) 99–108.